AGU PUBLICATIONS

Geophysical Research Letters

RESEARCH LETTER
10.1002/2015GL065985

Special Section:
First Results from the MAVEN Mission to Mars

Changes in the thermosphere and ionosphere of Mars from Viking to MAVEN

Paul Withers[1,2], Marissa Vogt[2], Paul Mahaffy[3], Mehdi Benna[3], Meredith Elrod[3], and Bruce Jakosky[4]

[1]Department of Astronomy, Boston University, Boston, Massachusetts, USA, [2]Center for Space Physics, Boston University, Boston, Massachusetts, USA, [3]Planetary Environments Laboratory, NASA Goddard Space Flight Center, Greenbelt, Maryland, USA, [4]Laboratory for Atmospheric and Space Physics, University of Colorado Boulder, Boulder, Colorado, USA

Abstract We compare Viking and Mars Atmosphere and Volatile EvolutioN mission (MAVEN) Neutral Gas and Ion Mass Spectrometer (NGIMS) observations of the thermosphere and ionosphere of Mars in order to test predictions of large variations in conditions over the solar cycle and with season. Substantial differences exist between the Viking observations at solar minimum and near aphelion and the MAVEN NGIMS observations at moderate solar activity and near perihelion. Differences in the O/CO_2 ratio, the O^+ ionospheric peak, ion densities at high altitude, and neutral and ion scale heights can be attributed to differences in solar activity and season, but the relative importance of solar activity and season for these differences was not established. Current models do not explain the observed differences in the mixing ratios of N, NO, and O_2. These results place new constraints on models of how the thermosphere and ionosphere of Mars vary over the solar cycle and with season.

Key Points:
- Vertical structure of the thermosphere above 250 km differs significantly from expectations
- Exobase altitude differs greatly from Viking to MAVEN
- Gross chemical composition similar from Viking to MAVEN

Correspondence to:
P. Withers,
withers@bu.edu

Citation:
Withers, P., M. Vogt, P. Mahaffy, M. Benna, M. Elrod, and B. Jakosky (2015), Changes in the thermosphere and ionosphere of Mars from Viking to MAVEN, *Geophys. Res. Lett.*, *42*, doi:10.1002/2015GL065985.

Received 31 AUG 2015
Accepted 23 SEP 2015

1. Introduction

Solar irradiance maintains the atmospheres of the solar system. Conditions at tropospheric altitudes are controlled by the visible portion of the solar spectrum, which is very stable over time. By contrast, composition, dynamics, and temperature at thermospheric and ionospheric altitudes are controlled by the extreme ultraviolet and soft X-ray portion of the spectrum. This irradiance is highly variable on time scales of minutes to hours due to solar flares, days to weeks due to the solar rotation, and years due to the 11 year solar cycle [*Lean*, 1987, 1991]. Consequently, thermospheric and ionospheric conditions are expected to vary significantly on a range of time scales. Since the irradiance at ionizing wavelengths shortward of 90 nm doubles from solar minimum to solar maximum [*Girazian and Withers*, 2015], variations over the course of the 11 year solar cycle are predicted to be large. Upper atmospheric conditions are also predicted to vary with season, which includes changes in both subsolar latitude caused by obliquity and heliocentric distance caused by orbital eccentricity.

In regard to the atmosphere of Mars, *Bougher et al.* [2015] predicted that the midafternoon thermospheric temperature at 200 km practically doubles from solar minimum to solar maximum. They also predicted that the altitude at which neutral atomic oxygen takes over from neutral carbon dioxide as the dominant species increases by 40 km from solar minimum to solar maximum. *Valeille et al.* [2009] predicted that the density of neutral atomic oxygen at 165 km and the escape rate of suprathermal neutral atomic oxygen double from solar minimum to solar maximum. *González-Galindo et al.* [2009] predicted that the midafternoon thermospheric temperature at a pressure level of 10^{-6} Pa doubles from solar minimum to solar maximum. *Krasnopolsky* [2002] predicted that the ionospheric electron density at 250 km increases by an order of magnitude from solar minimum to solar maximum. A similar increase was also predicted by *Fox* [2015].

González-Galindo et al. [2009] predicted that the altitude at which neutral atomic oxygen takes over from neutral carbon dioxide as the dominant species changes by 40 km over a Mars year and that the O/CO_2 ratio at the 1.4×10^{-4} Pa pressure level (~150 km) varies by a factor of 4 over a Mars year. *González-Galindo et al.* [2013] predicted that the altitude of ionospheric peak at the subsolar point changes by over a scale height over a Mars year, and the corresponding peak density changes by over 20%. *Chaufray et al.* [2014] predicted that the O^+ density at 200 km altitude above the subsolar point changes by a factor of 4 over a Mars year. Furthermore, geographic location may also affect upper atmospheric conditions, particularly those that are influenced by interactions with the solar wind and magnetosphere [e.g., *Ma et al.*, 2004].

Accurate predictions of variations in atmospheric composition over the seasons and the solar cycle are important for understanding the behavior of present-day Mars and for determining the state of the planet's atmosphere and climate in the ancient past. This is especially true for the O/CO_2 ratio, since CO_2 is the dominant species at low altitudes and O is the dominant species at high altitudes. Neutral atomic oxygen plays a crucial role in the aeronomy of the thermosphere and ionosphere of Mars [*Chamberlain and Hunten*, 1987; *Barth et al.*, 1992; *Mendillo et al.*, 2002; *Nagy*, 2008]. It is one of the most abundant species in the thermosphere and exosphere. It affects the efficiency of CO_2 15 μm radiative cooling. The abundance of O in the upper atmosphere helps to understand why CO_2 is surprisingly stable against losses due to dissociation by the absorption of photons and the impacts of suprathermal electrons. It is responsible for conversion of the primary photo-produced ion, CO_2^+, into the most abundant ion, O_2^+. Many pathways for the escape of oxygen atoms to space involve neutral oxygen-bearing species. Of these species, atomic oxygen is the most abundant in the thermospheric reservoir from which escape occurs.

For almost four decades, the only measurements of the vertical structure of the composition of the thermosphere and ionosphere of Mars have been the two Viking Lander profiles. With essentially no other compositional measurements available for either the thermosphere or the ionosphere, understanding of how the neutral and ion compositions change over the solar cycle and seasons has been poorly constrained and hence highly uncertain. This situation changed with the arrival of the Mars Atmosphere and Volatile EvolutioN mission (MAVEN) spacecraft at Mars on 22 September 2014. The MAVEN payload includes the Neutral Gas and Ion Mass Spectrometer (NGIMS) [*Mahaffy et al.*, 2014], which measures the densities of neutral and ionized species in the upper atmosphere and exosphere of Mars when the spacecraft descends to low altitudes on periapsis passes.

Due to differences in solar irradiance, season, and geographic location, thermospheric and ionospheric conditions are expected to be different between the Viking and MAVEN observations. The aims of this article are to report how thermospheric and ionospheric compositions changed between the Viking and MAVEN NGIMS observations and to draw conclusions from these findings about the aeronomy of Mars. These aims will be achieved by presenting both sets of thermospheric and ionospheric observations, then identifying and interpreting the major differences between them. Section 2 describes the Viking and MAVEN NGIMS thermospheric and ionospheric observations. Section 3 compares these two sets of thermospheric observations, and section 4 compares these two sets of ionospheric observations. Section 5 summarizes the conclusions of this work.

2. Description of Observations

Viking Lander 1 and 2 measured vertical profiles of thermospheric and ionospheric composition during their descents to the surface of Mars on 20 July 1976 (23°N, Ls = 97°, local solar time 16:13) and 3 September 1976 (48°N, Ls = 118°, local solar time 09:49), respectively [*Seiff and Kirk*, 1977]. Both these dates are near the start of northern summer and near aphelion, and both profiles were measured at solar zenith angles near 45° during solar minimum conditions ($F_{10.7}$ at Earth ≈70, ftp://ftp.ngdc.noaa.gov/STP/space-weather/solar-data/solar-features/solar-radio/noontime-flux/penticton/penticton_adjusted/listings/listing_drao_noontime-flux-adjusted_monthly.txt).

For MAVEN NGIMS, data from inbound and outbound legs of periapsis passes were used for ionospheric species, but only data from the inbound legs of periapsis passes were used for neutral species. This was because neutral atomic oxygen measurements on the outbound legs of periapsis passes require more sophisticated processing that has not yet been completed [*Mahaffy et al.*, 2015]. Even so, additional processing was required for the inbound neutral atomic oxygen measurements, since the instrumental background is relatively large for this species even in inbound measurements. We began with the original atomic oxygen densities, calculated the average density from 400 km to 450 km, and declared this to be the relevant instrumental background. Adjusted oxygen densities were calculated by subtracting this background from the original densities. Nevertheless, the adjusted atomic oxygen densities were still not acceptable at high altitudes and adjusted atomic oxygen densities above 250 km were replaced by an exponential extrapolation of densities between 200 km and 250 km.

The ionospheric data come from February 2015 to May 2015 (Ls = 299°–348° of Mars Year 32), when solar activity was moderate ($F_{10.7}$ at Earth ≈140) and the planet was near perihelion (1.42–1.53 AU). One hundred and two orbits of data are used that cover latitudes 60°S–40°N and local solar times 8–16 h. Due to the

restriction to inbound legs, the neutral data come from May 2015 (Ls = 339° – 348° of Mars Year 32), when solar activity was moderate ($F_{10.7}$ at Earth ≈140). Thirty-six orbits of data are used that cover latitudes 60°S – 40°S and local solar times 7 – 9 h.

MAVEN NGIMS data were acquired at many different solar zenith angles. In order to compare the MAVEN NGIMS data to Viking, for each species we select all measurements between 45° and 60° solar zenith angle. We further divide these measurements into 10 km vertical bins. For each species and each 10 km vertical bin, we find the median density. Since the data set includes a range of latitudes, seasons, and solar irradiances, it is not necessary to use a narrower solar zenith angle range. Reducing the solar zenith angle range does not significantly decrease the scatter in density for a given species and altitude.

The formal 1σ uncertainty in an individual MAVEN NGIMS density measurement is 20%. Since some of the contributions to that uncertainty are systematic, not random, a similar uncertainty should be assigned to the median densities reported here. Furthermore, MAVEN NGIMS ion densities are calibrated by normalizing the sum of the count rate of all ions to the electron density measured by the Langmuir Probe and Waves instrument. This calibration was performed in the first few weeks of the mission [*Benna et al.*, 2015], and the possibility of drifts in the calibration is still being assessed. To provide a sense of the variability in the data, lower and upper quartiles are also reported.

2.1. Thermospheric Observations

The Viking neutral mass spectrometer measured densities of six neutral species (CO_2, N_2, CO, O_2, NO, and Ar), as shown in Figure 1a [*Nier and McElroy*, 1977]. Inconveniently, Ar was omitted from this figure by the original authors — its abundance is approximately 2% that of CO_2. Separate abundances of N_2 and CO, both of which have masses of 28 amu, were determined by analysis of mass peaks attributed to fragments of the original molecules. The instrumental range spanned masses 1 to 49 amu. In addition to the aforementioned species, *Nier and McElroy* [1977] found that the mixing ratios of H_2 and He were less than 10^{-4} at the low altitudes where instrumental sensitivity was greatest. They also inferred that O must be present in the atmosphere but stated that "a quantitative determination of atomic oxygen has not been possible as yet owing to uncertainties in the extent to which gas may be removed on surfaces of the instrument." Chemical models constrained by these neutral data and simultaneous ion composition data acquired by a retarding potential analyzer suggested that the abundance of O was significant and that it becomes the most abundant species above 200 km altitude. *Chen et al.* [1978] predicted that the density of O decreases exponentially with increasing altitude with a scale height of 30 km and a density at 200 km of 3.5×10^7 cm^{-3}.

The MAVEN NGIMS neutral density profiles are shown in Figure 1b. The density profiles are shown to be 400 km, a much higher altitude than the Viking data, which do not extend above 200 km. The basic composition is similar to that observed by Viking — and, in the case of O, inferred by Viking. CO_2 is the most abundant species at low altitudes, with O taking over at higher altitudes. Although O is the most abundant species at high altitudes, the abundances of the other species are not negligible, as can be seen from a comparison of the O and total densities in this figure. Above 250 km, the abundances of the nonnegligible species CO_2, CO/N_2, N, and O_2 are all quite similar. Species detected include masses 4 (He), 14 (N), 16 (O), 28 (CO and N_2), 30 (NO), 32 (O_2), 40 (Ar), and 44 (CO_2). At high altitudes, the abundance of NO (mass 30) decreases with altitude with a scale height that is surprisingly similar to that for He (mass 4).

2.2. Ionospheric Observations

The Viking lander ion composition measurements, which are shown in Figure 1c, extend from 120 km to almost 300 km with a vertical resolution of 5 km. The minimum reported ion density was on the order of 100 cm^{-3}. The main features of these profiles were summarized in *Withers et al.* [2015]. Models that reproduce these observations and extend to higher altitudes generally predict a topside composition dominated by O_2^+ and relatively slow decreases in O^+, O_2^+, and CO_2^+ ion density with increasing altitude above 250 km [e.g., *Chen et al.*, 1978; *Fox*, 2015].

The MAVEN NGIMS ion density profiles are shown in Figure 1d. The density profiles extend to 500 km, a much higher altitude than the Viking data, which do not extend above 300 km. The main features of these profiles were summarized in *Withers et al.* [2015].

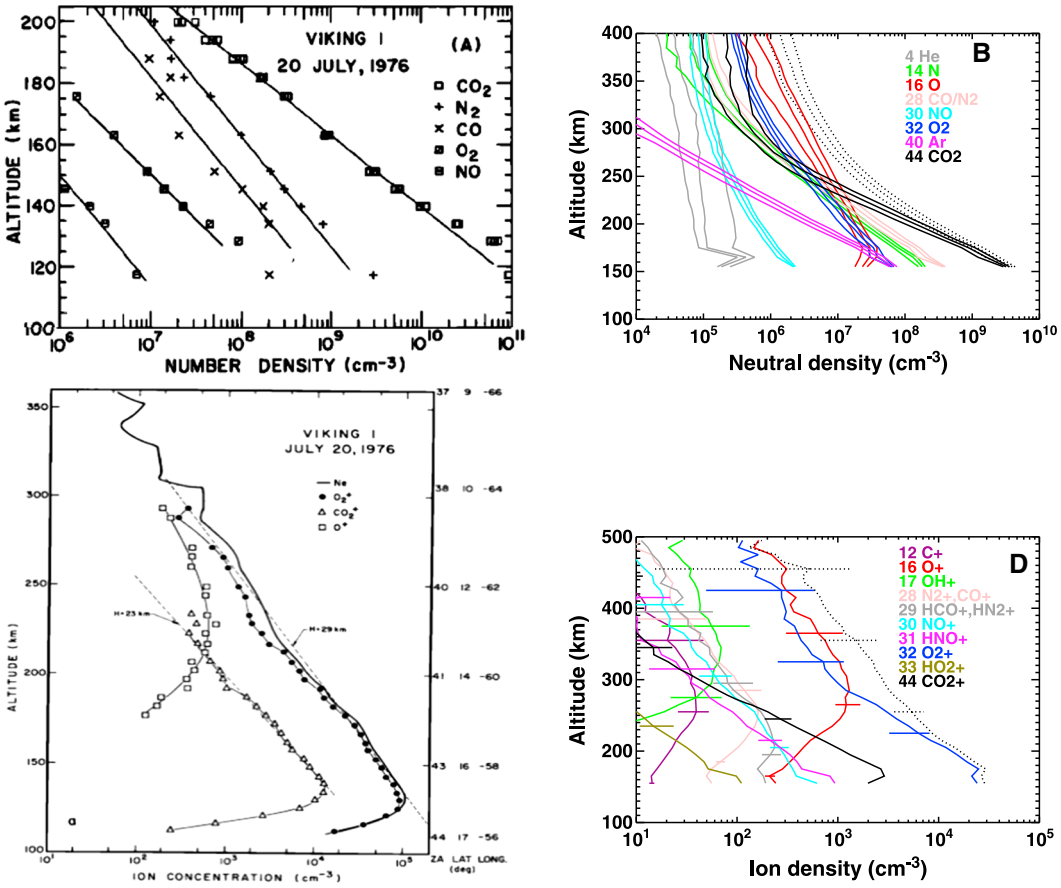

Figure 1. (a) Viking Lander 1 measurements of the number densities of neutral CO_2, N_2, CO, O_2, and NO. Ar was also measured, but is not shown. Its mixing ratio is approximately 2% that of CO_2. Neutral atomic oxygen could not be measured by this instrument. Figure 4 of *Nier and McElroy* [1977], reproduced by permission of American Geophysical Union. (b) MAVEN NGIMS measurements of neutral densities between solar zenith angles of 45° and 60°. Species are indicated by color, as shown on the figure. The total number density is shown by the dotted black line. Median, lower quartile, and upper quartile values are shown for each species. (c) Viking Lander 1 measurements of the number densities of O^+, O_2^+, and CO_2^+ ions. Figure 6 of *Hanson et al.* [1977], reproduced by permission of American Geophysical Union. (d) MAVEN NGIMS measurements of ion densities between solar zenith angles of 45° and 60°. Species are indicated by color as shown. The total ion density is shown by the dotted black line. Median values are shown. The lower and upper quartile values are illustrated for each species at several altitudes by horizontal lines.

3. Comparison of Thermospheric Observations

Figure 2a, which compares the Viking and MAVEN NGIMS thermospheric composition data, illustrates the main similarities and differences between them, and Figure 2b shows the thermospheric composition at 200 km as measured by Viking and MAVEN NGIMS.

The mixing ratios of mass 28 species CO and N_2, Ar, and CO_2 are similar in the two data sets. At present, MAVEN NGIMS data processing has yielded the total abundance of the two mass 28 species CO and N_2. The separate abundances of these species will be determined later as the data processing progresses further, as was done for Viking [*Nier and McElroy*, 1977]. The small He mixing ratio in the MAVEN NGIMS observations is roughly consistent with the upper limit reported by the Viking investigators. The main differences between the Viking and MAVEN NGIMS thermospheric mixing ratios are that the O_2 mixing ratio is more than an order of magnitude smaller in the Viking observations than in the MAVEN NGIMS observations, the NO mixing ratio is about 5 times smaller in the Viking observations than in the MAVEN NGIMS observations, the O mixing ratio is about 6 times greater in the Viking observations than in the MAVEN NGIMS observations, and N, which has a mixing ratio of 0.1 in the MAVEN NGIMS observations, was not detected by Viking.

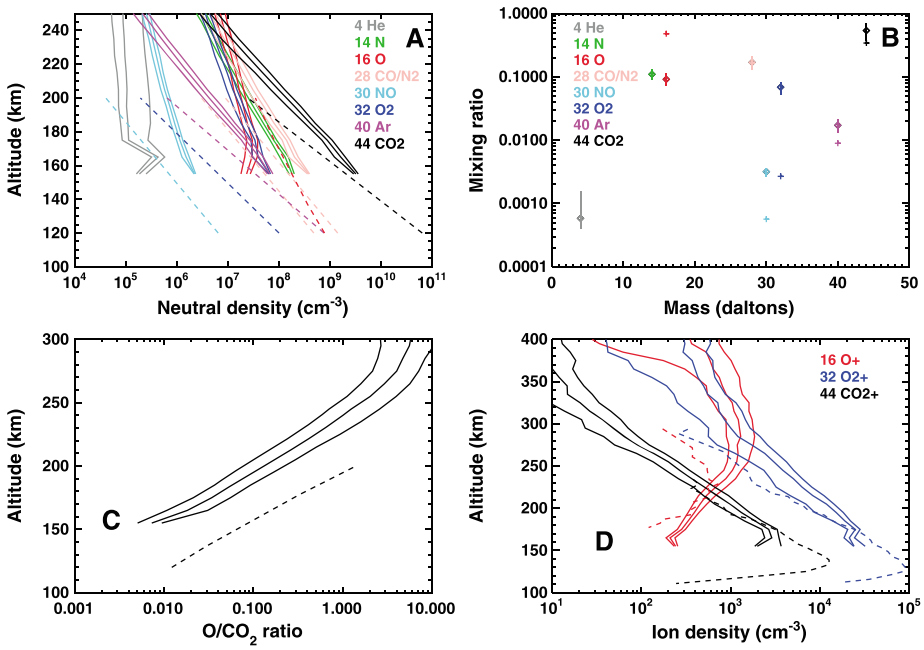

Figure 2. (a) Direct comparison of neutral densities measured by Viking Lander 1 (dashed lines) and MAVEN NGIMS (solid lines). Species are indicated by color as shown. Median, lower quartile, and upper quartile values are shown for MAVEN NGIMS densities. (b) Mixing ratios of neutral species at 200 km as measured by Viking Lander 1 (crosses) and MAVEN NGIMS (diamonds). Colors as shown. The lower (upper) end of each vertical line indicates the ratio of the lower (upper) quartile density of that species to the median total number density. (c) O/CO_2 ratio inferred from Viking Lander 1 data (dashed line) and measured by MAVEN NGIMS (solid line). The three solid lines show the ratios of the O lower quartile density to the CO_2 upper quartile density, the O median density to the CO_2 median density, and the O upper quartile density to the CO_2 lower quartile density. (d). Direct comparison of O^+, O_2^+, and CO_2^+ densities measured by Viking Lander 1 (dashed lines) and MAVEN NGIMS (solid lines). Species are indicated by color as shown. Median, lower quartile, and upper quartile values are shown for MAVEN NGIMS densities.

Although the Viking thermospheric observations do not extend above 200 km, many models have been developed that reach higher altitudes and are consistent with the available Viking observations [e.g., *Krasnopolsky*, 2002; *Bougher et al.*, 2015; *Fox*, 2015]. Such models have predicted that the high-altitude composition is dominated by O, CO_2, or both. However, in the MAVEN NGIMS observations, densities of N, O, mass 28 species (CO and N_2), and O_2 are within a factor of a few of each other between 200 km and 400 km, and the density of CO_2 is also similar to the densities of these species above 250 km. At 300 km, the densities of most of these species are between 3×10^5 and 1×10^6 cm^{-3}. The chemical composition of the upper atmosphere is not dominated by a single species or even a couple of species. Furthermore, the observed densities of N, NO, and O_2 are significantly greater than pre-MAVEN expectations [*Fox*, 2015; *Bougher et al.*, 2015].

These compositional differences at and above 200 km are unlikely to be the result of differences in solar activity and heliocentric distance, since they also exist with respect to model simulations at solar maximum as well as solar minimum. Instead, they indicate that current models of the thermosphere of Mars do not yet completely capture its chemistry.

The scale heights of neutral species are larger in the MAVEN NGIMS observations than in the Viking observations. The CO_2 scale height, for example, is 15 km in the MAVEN NGIMS observations and 10 km in the Viking Lander 1 observations, corresponding to temperatures of 270 K and 180 K, respectively. It is 7 km (120 K) in the more northerly Viking Lander 2 observations. These Viking temperatures were confirmed by the atmospheric structure investigations on the two Viking Lander [*Seiff and Kirk*, 1977]. The Viking Lander 2 temperature is colder than the Viking Lander 1 temperature due to its more poleward latitude. The warmer temperatures seen by MAVEN NGIMS are due to differences in the Mars-Sun distance and in the solar spectrum. Assuming a constant solar irradiance, the solar flux at the time of the MAVEN NGIMS observations and a Mars-Sun distance of 1.5 AU is 20% greater than that at the time of the Viking Lander 1 observations and a Mars-Sun distance of 1.65 AU. Moreover, the irradiance at fixed distance at the extreme ultraviolet wavelengths that heat and

ionize the thermosphere increased from Viking to MAVEN as solar activity advanced from minimum to moderate ($F_{10.7}$ at Earth ≈70 to 140).

The exobase altitude is higher in the MAVEN NGIMS observations than in the Viking observations. The exobase altitude z_{exo} satisfies the following:

$$\sigma_C \int_{z=z_{exo}}^{z=\infty} n(z)\mathrm{d}z = 1 \quad (1)$$

Here n is the neutral number density, z is altitude, and σ_C is the collision cross section, which equals 3×10^{-15} cm^2 for typical atmospheric species [*Chamberlain and Hunten*, 1987; *Fox and Hać*, 2009]. Hence, the column density above the exobase equals 3×10^{14} cm^{-2}, which in the MAVEN NGIMS observations places the exobase around 200 km, an altitude at which CO_2 is the dominant neutral species. By contrast, the exobase altitude in the Viking observations is 180 km [*Mueller-Wodarg et al.*, 2008]. This can also be attributed to differences in the Mars-Sun distance and in the solar activity.

As previously noted, the O/CO_2 ratio is critically important for the aeronomy of the thermosphere and ionosphere of Mars. However, the abundance of neutral atomic oxygen is notoriously challenging to measure with mass spectrometers, because it readily adsorbs and recombines on instrumental surfaces [*Nier and McElroy*, 1977; *Hanson et al.*, 1977]. Consequently, the Viking investigators inferred the abundance of neutral atomic oxygen, which could not be directly measured, indirectly using chemical models constrained by simultaneous Viking neutral and ion density data [*Chen et al.*, 1978]. Current mass spectrometers, such as MAVEN NGIMS, are better able to measure neutral atomic oxygen. The O/CO_2 ratios inferred by Viking and measured by MAVEN NGIMS are shown in Figure 2c as functions of altitude. Densities of the two species are equal at 240 km in the MAVEN NGIMS data and 200 km in the Viking data. The MAVEN NGIMS O/CO_2 ratio increases exponentially with altitude between 170 km and 270 km with a scale height of 17 km. At altitudes where both spacecraft acquired data, the MAVEN NGIMS ratio is an order of magnitude smaller than the Viking ratio. The somewhat counter-intuitive result that higher solar activity, which might be expected to enhance the photodissociation of CO_2, causes a smaller O/CO_2 ratio is supported by theoretical predictions [*Bougher et al.*, 2000].

Bougher et al. [2000] reported simulated values of the O/CO_2 ratio for Ls = 270° and moderate solar activity at 15 h local solar time, conditions that are similar to those experienced by MAVEN NGIMS. At 160–200 km, the MAVEN NGIMS O/CO_2 ratio is half the predicted ratio. Differences of this magnitude are not surprising. Models and data both show significant changes in the O/CO_2 ratio with altitude, so comparisons at fixed altitude can be biased by expansion or contraction of the lower atmosphere. Even at a fixed pressure level, seasonal variations may be significant. *González-Galindo et al.* [2009] predicted that the O/CO_2 ratio at the 1.4×10^{-4} Pa pressure level (∼150 km) varies by a factor of 3 from Ls = 270° to 360°. The magnitude of the observed differences in the O/CO_2 ratio between MAVEN NGIMS observations, values inferred from Viking, and predictions, though large, are therefore consistent with plausible variations with altitude, season, and solar activity. They do not necessarily indicate gaps in the present understanding of the chemistry of atomic oxygen on Mars.

Although the MAVEN NGIMS data do not extend low enough to reach the ionospheric peak, the altitude of the peak can be estimated from the neutral densities. It is generally considered that the ionospheric peak occurs at an optical thickness of one for ionizing EUV photons in a carbon dioxide atmosphere [*Chamberlain and Hunten*, 1987]. That is,

$$\sum_j \sigma_{I,j} \int_{z=z_{pk}}^{z=\infty} n_j(z)\mathrm{d}z = \cos(\mathrm{SZA}) \quad (2)$$

Here the subscript j labels the neutral species, σ_I is the ionization cross section, z_{pk} is the altitude of the ionospheric peak, and SZA is solar zenith angle. In this case, we may assume that neutral densities vary exponentially with altitude and that CO_2 is the dominant neutral species. Thus,

$$\sigma_{I,CO2}\, n_{CO2}\left(z_{pk}\right)\, H = \cos(\mathrm{SZA}) \quad (3)$$

The relevant ionization cross section is 3×10^{-17} cm^2 for CO_2 [*Ma et al.*, 2004; *Withers*, 2009].

As before, H = 15 km. For solar zenith angles of 45° to 60°, the CO_2 number densities at the ionospheric peak are 1.6 to 1.1×10^{10} cm^{-3}, which occur at 132–137 km. These predicted peak altitudes are consistent

with the range observed by other instruments [*Morgan et al.*, 2008; *Němec et al.*, 2011; *Fallows et al.*, 2015]. Since these previous observations span a wide range of latitudes, seasons, and solar activity levels, it is not surprising that the peak altitude inferred from MAVEN NGIMS thermospheric measurements is consistent with them. This result implies that the assumption that the ionospheric peak occurs at an optical thickness close to 1 is reasonable. However, the inferred peak altitude is higher than the values reported by *Hantsch and Bauer* [1990]. We attribute this difference to changes in the reference areoid from the Viking era to the post-Mars Global Surveyor era [*Withers and Pratt*, 2013].

4. Comparison of Ionospheric Observations

Figure 2d compares the Viking and MAVEN NGIMS O^+, O_2^+, and CO_2^+ densities, which illustrate the main similarities and differences between them. The Viking observations left the ionospheric composition above 300 km tantalizingly unclear: does O^+ become dominant at high altitudes, does O_2^+ remain the most abundant, or do densities of the two species become similar? The MAVEN NGIMS observations show that densities of O^+ and O_2^+ are remarkably similar above 300 km. In both MAVEN NGIMS and Viking observations, the CO_2^+/O_2^+ ratio changes very slowly with altitude and O^+ is more abundant than CO_2^+ above 210–220 km. However, there are some substantial differences between the Viking and MAVEN NGIMS observations. The peak O^+ abundance is twice as large and 60 km higher in altitude in the MAVEN NGIMS observations than in the Viking observations. The O_2^+ and CO_2^+ density scale heights are 50% larger in the MAVEN NGIMS observations than in the Viking observations, although in both cases the O_2^+ scale height is about 25% larger than the CO_2^+ scale height. At 290 km, both O^+ and O_2^+ densities are about 6 times larger in the MAVEN NGIMS observations than in the Viking observations. The CO_2^+ densities in the two data sets are remarkably similar at 170–230 km, despite differences in the corresponding neutral densities and scale heights.

It is noteworthy that the neutral O/CO_2 ratio is larger for Viking than MAVEN NGIMS, but the O^+/CO_2^+ ratio is larger for MAVEN NGIMS than for Viking. This may be related to the role played by O in the destruction of CO_2^+ ions by charge exchange. The fact that both ion and neutral scale heights are 50% larger in MAVEN NGIMS data than in Viking data illustrates the close relationship that exists between the vertical structures of the ionized and neutral components of the upper atmosphere. As with the neutral scale heights, the ion scale heights are greater in MAVEN NGIMS data than in the Viking data due to differences in the Mars-Sun distance and in the solar activity.

Ion densities at fixed altitude are greater in MAVEN NGIMS data than in Viking data due to solar activity increasing from minimum to moderate and the heliocentric distance decreasing from near aphelion to near perihelion. This not only increases ionization rates, but it also causes the atmosphere to expand, which raises levels of fixed pressure and fixed optical thickness. The latter factor tends to increase ion densities at fixed altitude since ion densities decrease with decreasing optical thickness above the peak. Furthermore, increased solar activity increases the electron temperature, which decreases ion loss rates and increases ion densities.

Numerical models that allowed solar activity to change while heliocentric distance and electron temperature were held constant predicted changes in peak O^+ abundance and altitude, O_2^+ and CO_2^+ scale heights, and ion densities at 290 km over the solar cycle that are comparable to those reported here [*Krasnopolsky*, 2002; *Fox*, 2015].

The altitude above which the ionosphere is no longer in photochemical equilibrium and plasma transport can no longer be neglected and can be calculated from these data. At this transition altitude, the time constants for removal of plasma by chemical neutralization, τ_C, and by transport, τ_T, are equal. The location of this transition altitude is not merely important for delineating different ionospheric regions. Its location affects not only the amount of ionospheric plasma that can be stripped away by certain escape processes but also the amount of plasma that may flow across the terminator from the dayside to the nightside, which is one of the primary mechanisms that sustains nightside plasma densities. At higher altitudes, plasma is susceptible to escape by ion outflow and to transterminator flow from the dayside to the nightside.

Anticipating the eventual result, we assume that this transition altitude occurs at an altitude where O_2^+ is the dominant ion and CO_2 is the dominant neutral, which leads to the following expressions.

$$\tau_C = \frac{1}{\alpha_{DR} N_i} \tag{4}$$

$$\tau_T = \frac{H^2 m_i \nu_{\text{in}}}{k_B \left(T_e + T_i\right)} \tag{5}$$

This expression for τ_T is derived under certain idealized assumptions regarding the plasma velocity [*Rishbeth and Garriott*, 1969; *Schunk and Nagy*, 2009], but is sufficient for an initial evaluation of the situation. In equations (4) and (5), α_{DR} is the rate coefficient for the dissociative recombination of an O_2^+ ion with an electron, N_i is the O_2^+ density, H is the neutral scale height, m_i is the mass of an O_2^+ ion, ν_{in} is the ion-neutral collision frequency, k_B is the Boltzmann constant, T_e is the electron temperature, and T_i is the ion temperature. From *Schunk and Nagy* [2009], $\alpha_{\text{DR}} = 2.4 \times 10^{-7} \left(300\text{K}/T_e\right)^{0.7}$. As noted previously, H is 10 km for Viking and 15 km for MAVEN NGIMS. From *Banks and Kockarts* [1973], ν_{in} is proportional to the CO_2 number density as specified in equation (56) of *Withers* [2008]. We assume representative uniform values for T_e and T_i of 1500 K and 500 K, respectively [*Chen et al.*, 1978; *Hanson et al.*, 1977; *Hanson and Mantas*, 1988]. The numerical values are consistent with Viking data and initial interpretation of MAVEN observations (R. Lillis, personal communication, 2015), but the assumption of uniform values is not particularly realistic. However, τ_C increases exponentially with altitude due to the exponential decrease of N_i with altitude and τ_T decreases exponentially with altitude due to the exponential decrease of ν_{in} and the neutral density with increasing altitude. Given these trends, the inferred altitude at which $\tau_C = \tau_T$ is not very sensitive to crude assumptions concerning T_e and T_i. With these assumptions, the altitude at which $\tau_C = \tau_T$ is one scale height higher in the MAVEN NGIMS observations (170 km) than in the Viking observations (155 km).

5. Summary and Conclusions

Substantial differences exist between thermospheric and ionospheric conditions observed at similar solar zenith angles by Viking Lander 1 and MAVEN NGIMS.

In the thermosphere, neutral scale heights are 50% greater in the MAVEN NGIMS observations than in the Viking observations. The exobase is 1–2 scale heights higher in the MAVEN NGIMS observations than in the Viking observations. The O/CO_2 ratio is an order of magnitude smaller in the MAVEN NGIMS observations than in the Viking observations. These differences can be attributed to solar activity levels increasing from minimum at the time of the Viking observations to moderate at the time of the MAVEN NGIMS observations, coincident with the Mars-Sun distance decreasing from near aphelion to near perihelion. However, compositional differences concerning the abundances of N, NO, and O_2, which are larger in the MAVEN NGIMS observations than in the Viking observations, and the number of species that contribute significantly to the total number density at high altitudes, which is larger in the MAVEN NGIMS observations than in the Viking observations, cannot be explained by these factors. Instead, they indicate that current models of the thermosphere of Mars do not yet completely capture its chemistry.

In the ionosphere, both O^+ and O_2^+ densities at 290 km are about 6 times larger in the MAVEN NGIMS observations than in the Viking observations. The peak O^+ abundance is twice as large and 60 km higher in altitude in the MAVEN NGIMS observations than in the Viking observations. The scale heights that describe the change in O_2^+ and CO_2^+ density with altitude are 50% larger in the MAVEN NGIMS observations than in the Viking observations. The altitude above which the ionosphere is no longer in photochemical equilibrium and plasma transport can no longer be neglected is one scale height higher in the MAVEN NGIMS observations than in the Viking observations. These differences can also be attributed to solar activity levels increasing from minimum at the time of the Viking observations to moderate at the time of the MAVEN NGIMS observations, coincident with the Mars-Sun distance decreasing from near aphelion to near perihelion.

Many thermosphere-ionosphere models have been developed to reproduce the Viking observations. Those models that are also successful at reproducing the MAVEN NGIMS observations reported here will be useful for elucidating the physical processes that determine the chemical compositions of the thermosphere and ionosphere, for describing how the thermosphere and ionosphere of Mars vary over the solar cycle and with season and for predicting conditions in the past. Those that are not will not.

Acknowledgments
We acknowledge Marie-Eve Gagne and Francisco Gonzalez-Galindo for helpful reviews. P.W. and M.V. were supported, in part, by NASA award NNX13AO35G. P.W. thanks Yingjuan Ma for providing Viking Lander 1 ion density data and Zachary Girazian for helpful discussions. MAVEN data are available from the NASA Planetary Data System (http://pds.nasa.gov). The MAVEN project is supported by NASA through the Mars Exploration Program.

The Editor thanks Francisco Gonzalez Galindo and Marie-Eve Gagne for their assistance in evaluating this paper.

References

Banks, P. M., and G. Kockarts (1973), *Aeronomy*, Academic Press, New York.

Barth, C. A., A. I. F. Stewart, S. W. Bougher, D. M. Hunten, S. J. Bauer, and A. F. Nagy (1992), Aeronomy of the current Martian atmosphere, in *Mars*, edited by H. H. Kieffer et al., pp. 1054–1089, Univ. of Arizona Press, Arizona.

Benna, M., P. R. Mahaffy, J. M. Grebowsky, J. L. Fox, R. V. Yelle, and B. M. Jakosky (2015), First measurements of composition and dynamics of the Martian ionosphere by MAVEN's Neutral Gas and Ion Mass Spectrometer, *Geophys. Res. Lett.*, *42*, doi:10.1002/2015GL066146.

Bougher, S. W., S. Engel, R. G. Roble, and B. Foster (2000), Comparative terrestrial planet thermospheres 3. Solar cycle variation of global structure and winds at solstices, *J. Geophys. Res.*, *105*, 17,669–17,692, doi:10.1029/1999JE001232.

Bougher, S. W., D. Pawlowski, J. M. Bell, S. Nelli, T. McDunn, J. R. Murphy, M. Chizek, and A. Ridley (2015), Mars global ionosphere-thermosphere model: Solar cycle, seasonal, and diurnal variations of the Mars upper atmosphere, *J. Geophys. Res. Planets*, *120*, 311–342, doi:10.1002/2014JE004715.

Chamberlain, J. W., and D. M. Hunten (1987), *Theory of Planetary Atmospheres*, 2nd ed., Academic Press, New York.

Chaufray, J.-Y., F. Gonzalez-Galindo, F. Forget, M. Lopez-Valverde, F. Leblanc, R. Modolo, S. Hess, M. Yagi, P.-L. Blelly, and O. Witasse (2014), Three-dimensional Martian ionosphere model: II. Effect of transport processes due to pressure gradients, *J. Geophys. Res. Planets*, *119*, 1614–1636, doi:10.1002/2013JE004551.

Chen, R. H., T. E. Cravens, and A. F. Nagy (1978), The Martian ionosphere in light of the Viking observations, *J. Geophys. Res.*, *83*, 3871–3876.

Fallows, K., P. Withers, and M. Matta (2015), An observational study of the influence of solar zenith angle on properties of the M1 layer of the Mars ionosphere, *J. Geophys. Res. Space Physics*, *120*, 1299–1310, doi:10.1002/2014JA020750.

Fox, J. L. (2015), The chemistry of protonated species in the Martian ionosphere, *Icarus*, *252*, 366–392, doi:10.1016/j.icarus.2015.01.010.

Fox, J. L., and A. B. Hać (2009), Photochemical escape of oxygen from Mars: A comparison of the exobase approximation to a Monte Carlo method, *Icarus*, *204*, 527–544, doi:10.1016/j.icarus.2009.07.005.

Girazian, Z., and P. Withers (2015), An empirical model of the extreme ultraviolet solar spectrum as a function of $F_{10.7}$ based on TIMED-SEE data, *J. Geophys. Res. Space Physics*, *120*, 6779–6794, doi:10.1002/2015JA021436.

González-Galindo, F., F. Forget, M. A. López-Valverde, M. Angelats i Coll, and E. Millour (2009), A ground-to-exosphere Martian general circulation model: 1. Seasonal, diurnal, and solar cycle variation of thermospheric temperatures, *J. Geophys. Res.*, *114*, E04001, doi:10.1029/2008JE003246.

González-Galindo, F., J.-Y. Chaufray, M. A. López-Valverde, G. Gilli, F. Forget, F. Leblanc, R. Modolo, S. Hess, and M. Yagi (2013), Three-dimensional Martian ionosphere model: I. The photochemical ionosphere below 180 km, *J. Geophys. Res. Planets*, *118*, 2105–2123, doi:10.1002/jgre.20150.

Hanson, W. B., and G. P. Mantas (1988), Viking electron temperature measurements—Evidence for a magnetic field in the Martian ionosphere, *J. Geophys. Res.*, *93*, 7538–7544.

Hanson, W. B., S. Sanatani, and D. R. Zuccaro (1977), The Martian ionosphere as observed by the Viking retarding potential analyzers, *J. Geophys. Res.*, *82*, 4351–4363.

Hantsch, M. H., and S. J. Bauer (1990), Solar control of the Mars ionosphere, *Planet. Space Sci.*, *38*, 539–542.

Krasnopolsky, V. A. (2002), Mars' upper atmosphere and ionosphere at low, medium, and high solar activities: Implications for evolution of water, *J. Geophys. Res.*, *107*(E12), 5128, doi:10.1029/2001JE001809.

Lean, J. (1987), Solar ultraviolet irradiance variations—A review, *J. Geophys. Res.*, *92*, 839–868, doi:10.1029/JD092iD01p00839.

Lean, J. (1991), Variations in the Sun's radiative output, *Rev. Geophys.*, *29*, 505–535, doi:10.1029/91RG01895.

Ma, Y., A. F. Nagy, I. V. Sokolov, and K. C. Hansen (2004), Three-dimensional, multispecies, high spatial resolution MHD studies of the solar wind interaction with Mars, *J. Geophys. Res.*, *109*, A07211, doi:10.1029/2003JA010367.

Mahaffy, P. R., et al. (2014), The neutral gas and ion mass spectrometer on the Mars atmosphere and volatile evolution mission, *Space Sci. Rev.*, doi:10.1007/s11214-014-0091-1.

Mahaffy, P. R., M. Benna, M. Elrod, R. V. Yelle, S. W. Bougher, S. W. Stone, and B. M. Jakosky (2015), Structure and composition of the neutral upper atmosphere of Mars from the MAVEN NGIMS investigation, *Geophys. Res. Lett.*, *42*, doi:10.1002/2015GL065329.

Mendillo, M., A. Nagy, and J. H. Waite (2002), *Atmospheres in the Solar System: Comparative aeronomy*, AGU, Washington, D. C.

Morgan, D. D., D. A. Gurnett, D. L. Kirchner, J. L. Fox, E. Nielsen, and J. J. Plaut (2008), Variation of the Martian ionospheric electron density from Mars Express radar soundings, *J. Geophys. Res.*, *113*, A09303, doi:10.1029/2008JA013313.

Mueller-Wodarg, I. C. F., D. F. Strobel, J. I. Moses, J. H. Waite, J. Crovisier, R. V. Yelle, S. W. Bougher, and R. G. Roble (2008), Neutral atmospheres, *Space Sci. Rev.*, *139*, 191–234, doi:10.1007/s11214-008-9404-6.

Nagy, A. F. (2008), Preface, *Space Sci. Rev.*, *139*, 1–2, doi:10.1007/s11214-008-9353-0.

Nier, A. O., and M. B. McElroy (1977), Composition and structure of Mars' upper atmosphere—Results from the neutral mass spectrometers on Viking 1 and 2, *J. Geophys. Res.*, *82*, 4341–4349.

Němec, F., D. D. Morgan, D. A. Gurnett, F. Duru, and V. Truhlík (2011), Dayside ionosphere of Mars: Empirical model based on data from the MARSIS instrument, *J. Geophys. Res.*, *116*, E07003, doi:10.1029/2010JE003789.

Rishbeth, H., and O. K. Garriott (1969), *Introduction to Ionospheric Physics*, Academic Press, New York.

Schunk, R. W., and A. F. Nagy (2009), *Ionospheres*, 2nd ed., Cambridge Univ. Press, New York.

Seiff, A., and D. B. Kirk (1977), Structure of the atmosphere of Mars in summer at mid-latitudes, *J. Geophys. Res.*, *82*, 4364–4378.

Valeille, A., M. R. Combi, S. W. Bougher, V. Tenishev, and A. F. Nagy (2009), Three-dimensional study of Mars upper thermosphere/ionosphere and hot oxygen corona: 2. Solar cycle, seasonal variations, and evolution over history, *J. Geophys. Res.*, *114*, E11006, doi:10.1029/2009JE003389.

Withers, P. (2008), Theoretical models of ionospheric electrodynamics and plasma transport, *J. Geophys. Res.*, *113*, A07301, doi:10.1029/2007JA012918.

Withers, P. (2009), A review of observed variability in the dayside ionosphere of Mars, *Adv. Space Res.*, *44*, 277–307, doi:10.1016/j.asr.2009.04.027.

Withers, P., and R. Pratt (2013), An observational study of the response of the upper atmosphere of Mars to lower atmospheric dust storms, *Icarus*, *225*, 378–389.

Withers, P., et al. (2015), Comparison of model predictions for the composition of the ionosphere of Mars to MAVEN NGIMS data, *Geophys. Res. Lett.*, *42*, doi:10.1002/2015GL065205.